Volume 50 | Number 76 | 4 October 2014 | Pages 11065–11244

ChemComm

Chemical Communications

www.rsc.org/chemcomm

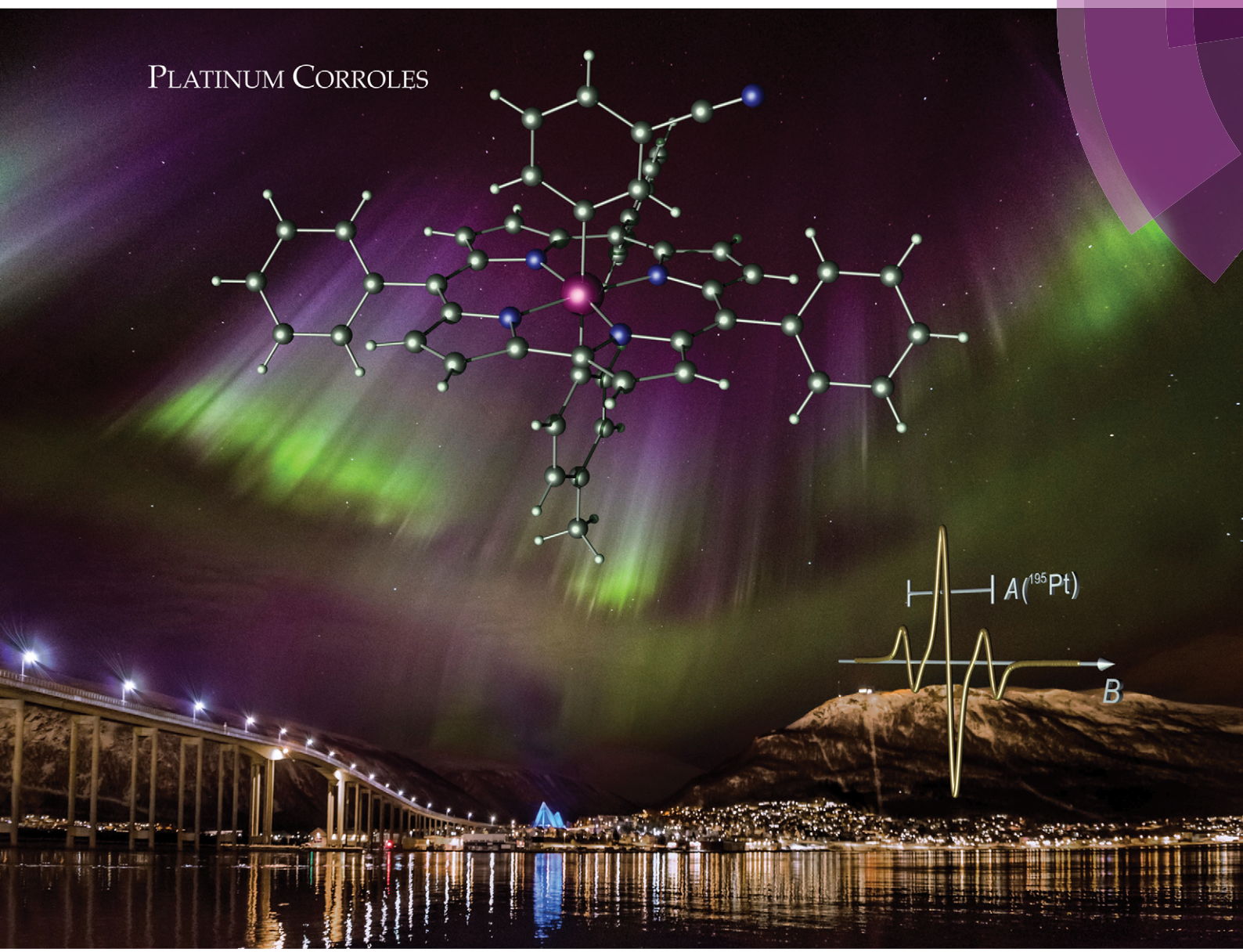

ISSN 1359-7345

ROYAL SOCIETY OF CHEMISTRY

COMMUNICATION

Abhik Ghosh *et al.*

Platinum corroles

ChemComm

COMMUNICATION

View Article Online
View Journal | View Issue

Platinum corroles†

Cite this: *Chem. Commun.*, 2014, 50, 11093

Received 7th April 2014,
Accepted 14th May 2014

DOI: 10.1039/c4cc02548b

www.rsc.org/chemcomm

Abraham B. Alemayehu,[a] Hugo Vazquez-Lima,[a] Christine M. Beavers,[b] Kevin J. Gagnon,[b] Jesper Bendix[c] and Abhik Ghosh*[a]

Platinum has been inserted into corroles for the first time and three oxidized Pt^{IV}(corrole$^{\bullet 2-}$)ArAr′ complexes have been structurally characterized. The Soret maxima of these complexes exhibit an unusually strong dependence on the *meso*-aryl substituents on the corrole, indicating aryl → corrole$^{\bullet 2-}$ charge transfer character in these transitions.

As trianionic ligands with contracted N_4 cores, corroles sustain a great deal of unique coordination chemistry relative to porphyrins.[1] Within this area, heavy element corroles are of particular interest as optical sensors, near-IR dyes, phosphors, and organic light emitting diodes.[2] The size mismatch between the corrole N_4 cores and the large ionic radii of the lower oxidation states of the 5d elements, however, poses formidable challenges for metal insertion. As of today, Hf,[3] W,[4] Re,[5] Ir,[6] and Au,[7] corroles have been synthesized, whereas others such as osmium and platinum corroles are still to be reported. Here we present unambiguous evidence, including multiple single-crystal X-ray analyses, for the formation of platinum corroles.

Insertion of Pt into corroles proved to be extraordinarily challenging. A large number of commercially available Pt precursors, each tested with a wide selection of solvents, failed to yield isolable Pt corrole derivatives. In the end, microwave irradiation of the commercially unavailable tetranuclear platinum acetate complex $[Pt(OAc)_2]_4{\cdot}2HOAc$[8] in benzonitrile at 140–150 °C for 2 hours led to low but reproducible yields (~6%) of diamagnetic Pt(IV) corroles. Notably, aerobic conditions were critical to the success of the reaction; strict exclusion of oxygen did not result in Pt-containing products. Based on MALDI-TOF mass spectrometry and ^{1}H NMR spectroscopy, the products could be formulated as Pt{T(*p*-X-Ph)C}(*o*/*m*/*p*-C_6H_4CN)(PhCN), where {T(*p*-X-Ph)C}$^{3-}$ is a *meso*-triarylcorrole trianion with aryl *para* substituents X = CF_3, H, CH_3, and OCH_3 and the axial benzonitrile-derived aryl ligand may be bound through the *o*-, *m*-, or *p*-carbon, relative to the CN group (Fig. 1). Thus, C–H activation of benzonitrile resulting in a Pt(IV)-aryl center has been critical to the synthesis of stable platinum corroles. Electrospray ionization mass spectrometric studies indicated the *N*-bound benzonitrile ligand in these Pt(IV) complexes to be labile. Preliminary X-ray analysis of the putative Pt{T(*p*-CF_3-Ph)C}(*m*-C_6H_4CN)(PhCN) complex indicated extensive disorder involving benzonitrile-derived ligands; despite some evidence of five-coordinate Pt{T(*p*-X-Ph)C}(*o*/*m*/*p*-C_6H_4CN), much of the material consisted of various regioisomers of Pt{T(*p*-X-Ph)C}(*o*/*m*/*p*-$C_6H_4CN)_2$, which formally correspond to a Pt(V) oxidation state. Thus, a second C–H activation, involving the *N*-coordinated benzonitrile, had taken place during crystallization. Air-stable, oxidized platinum complexes Pt{T(*p*-X-Ph)C}(*o*/*m*/*p*-C_6H_4CN)(*p*-$C_6H_4CH_3$) could be more

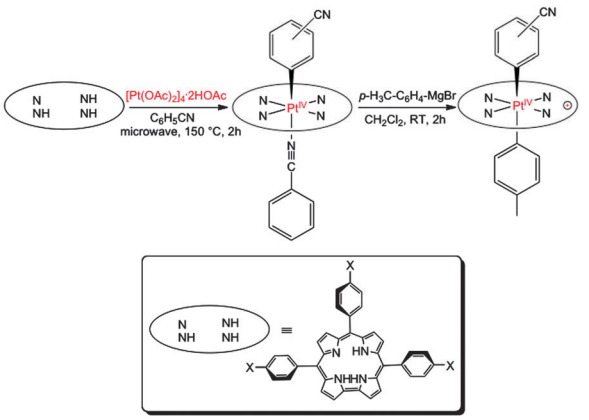

Fig. 1 Synthesis of six-coordinate Pt^{IV}–Ar corroles and oxidized Pt^{IV}–corrole$^{\bullet 2-}$–ArAr′ derivatives.

[a] *Department of Chemistry and Center for Theoretical and Computational Chemistry, UiT – The Arctic University of Norway, 9037 Tromsø, Norway. E-mail: abhik.ghosh@uit.no*
[b] *Advanced Light Source, Lawrence Berkeley National Laboratory, Berkeley, CA 94720-8229, USA*
[c] *Department of Chemistry, University of Copenhagen, Universitetsparken 5, DK-2100 Copenhagen, Denmark*

† Electronic supplementary information (ESI) available: Details of experimental procedures, spectra and X-ray structure determinations. CCDC 995762–995764. For ESI and crystallographic data in CIF or other electronic format see DOI: 10.1039/c4cc02548b

reliably obtained by treating the Pt(IV) complexes with an aryl-Grignard reagent (Fig. 1). Because of the low yields, only the *m*-C_6H_4CN regioisomers were fully characterized for all the corroles, whereas the *p*-C_6H_4CN isomer could be characterized for only one of the corroles. Fortunately, three oxidized Pt corroles yielded X-ray quality crystals, affording full structural characterization.

X-band EPR spectra were recorded for the oxidized Pt corroles in the solid state (Fig. 2), in solution (2 : 1 CH_2Cl_2 : toluene) at RT, and in a frozen glass at 73 K obtained from the same solution. The complexes all gave strong signals with *g*-values ~2.00, consistent with the ligand radical formulation Pt(corrole$^{\bullet 2-}$)ArAr′. The spectra could be simulated with fairly narrow linewidths (Lorentzian, fwhh = 3 G) and a slight *g*-anisotropy, but notably without any ^{195}Pt hyperfine coupling.[9] Upon dissolution in a mixture of CH_2Cl_2 and toluene at RT, the spectra changed profoundly (Fig. 3); the bandwidth became nearly twice as large, with concomitant appearance of fully resolved hyperfine coupling to ^{195}Pt. Freezing of the solution at 73 K had only a slight effect on the spectrum (Fig. 3). The much narrower signals in the solid state may be interpreted as an unusually well-behaved example of "exchange narrowing".[10] This is in agreement with the crystal structures, which indicate partial corrole π-stacking with relatively short interplanar distances of about 3.4 Å. The observed *g*-value range of 1.997–2.011 agrees with literature values for corrole-based radical complexes.[11] Although well-resolved in solution, the hyperfine coupling to Pt is too small for the radical to be Pt-centered.

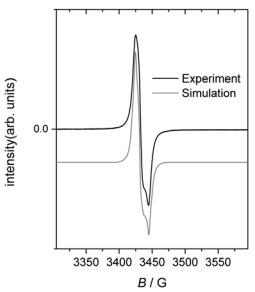

Fig. 2 Solid state, RT X-band EPR spectrum of Pt(TPC)(*m*-C_6H_4CN)(*p*-$C_6H_4CH_3$). Simulation offset for clarity. Simulation parameters: g = 1.999, 2.007, 2.011, value of $A(^{195}Pt)$ used = 0.8×10^{-3} cm^{-1}, Lorentzian bandshape, fwhh = 3.0 G.

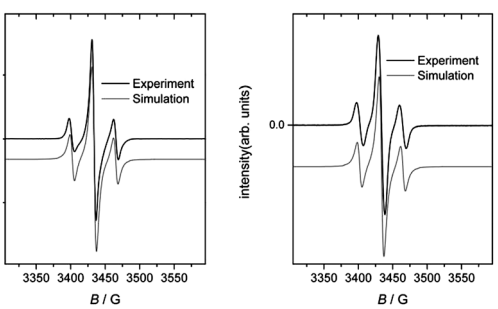

Fig. 3 Left: RT, solution, X-band EPR spectrum of Pt(TPC)(*m*-C_6H_4CN)(*p*-$C_6H_4CH_3$). Simulation offset for clarity. Simulation parameters: g = 2.005, $A(^{195}Pt) = 5.9 \times 10^{-3}$ cm^{-1}, Lorentzian bandshape, fwhh = 5.6 G. Right: frozen glass, 73 K spectrum of same solution. Simulation parameters: g = 2.005, $A(^{195}Pt) = 5.9 \times 10^{-3}$ cm^{-1}, Lorentzian bandshape, fwhh = 5.7 G.

Three of the oxidized Pt complexes Pt(TPC)(*m*-C_6H_4CN)(*p*-$C_6H_4CH_3$), Pt{T(*p*-CH_3-Ph)C}(*p*-C_6H_4CN)(*p*-$C_6H_4CH_3$), and Pt{T(*p*-CH_3-Ph)C}(*m*-C_6H_4CN)(*p*-$C_6H_4CH_3$) proved amenable to single-crystal X-ray analysis. All the structures refined well, giving R_1 [$I > 2\sigma(I)$] values ~3%. No evidence was found for counter-ions, positive or negative, consistent with the Pt^{IV}–corrole$^{\bullet 2-}$ formulation mentioned above. Selected bond distances are listed in Table 1 and a representative thermal ellipsoid plot is shown in Fig. 4. As for many metallocorroles,[12,13] the corrole macrocycles in all three complexes are almost perfectly planar. The short Pt–N distances of approximately 1.95 Å are consistent with a Pt(IV) oxidation state and the sterically constrained nature of the corrole N_4 core, while the axial Pt–C distances of about 2.1 Å are typical for unconstrained Pt^{IV}–C bond distances.

Fig. 5 depicts key results from DFT calculations on the model complexes Pt(corrole)(Ph)(PhCN) (C_s) and Pt(corrole)Ph_2 (C_{2v}). The optimized structural parameters are in excellent agreement with those observed experimentally (Table 1). To a first approximation, the spin density of Pt(corrole)Ph_2 corresponds to a corrole b_1 radical (in terms of C_{2v} irreps), which resembles a porphyrin a_{2u}-type radical,[14] *i.e.*, the spin density is largely localized on the three *meso* carbons and the four nitrogens and to a lesser extent on the direct C_β–C_β linkage. The Pt does not carry a significant amount of spin density, thereby ruling out any degree of Pt(V) character. Closer examination of Fig. 5 indicates that the corrole carries only about two-thirds of the total molecular spin density; the remaining one-third of the spin density is evenly divided between the two formally anionic phenyl *ipso* carbons. Thus, the HOMO is not a pure corrole b_1 HOMO, but has a certain amount of aryl character as well.

Table 2 presents redox potentials for Pt{T(*p*-X-Ph)C}(*m*-C_6H_4CN)(PhCN), the oxidized Pt{T(*p*-X-Ph)C}(*m*-C_6H_4CN)(*p*-P)C} complexes

Table 1 Pertinent bond distances for Pt{T(*p*-CH_3-Ph)C}(*p*-C_6H_4CN)(*p*-$C_6H_4CH_3$), Pt(TPC)(*m*-C_6H_4CN)(*p*-$C_6H_4CH_3$) and Pt{T(*p*-CH_3-Ph)C}(*m*-C_6H_4CN)(*p*-$C_6H_4CH_3$)

Pt{T(*p*-CH_3-Ph)C}(*p*-C_6H_4CN)(*p*-$C_6H_4CH_3$)		Pt(TPC)(*m*-C_6H_4CN)(*p*-$C_6H_4CH_3$)		Pt{T(*p*-CH_3-Ph)C}(*m*-C_6H_4CN)(*p*-$C_6H_4CH_3$)	
Pt1–N1	1.948(2)	Pt1–N1	1.942(3)	Pt1–N1	1.951(2)
Pt1–N2	1.9698(19)	Pt1–N2	1.965(3)	Pt1–N2	1.973(2)
Pt1–N3	1.9693(19)	Pt1–N3	1.970(3)	Pt1–N3	1.976(2)
Pt1–N4	1.9470(19)	Pt1–N4	1.945(3)	Pt1–N4	1.944(2)
Pt1–C_{ax}(41)	2.119(2)	Pt1–C_{ax}(38)	2.119(3)	Pt1–C_{ax}(41)	2.128(2)
Pt1–C_{ax}(48)	2.129(2)	Pt1–C_{ax}(45)	2.114(3)	Pt1–C_{ax}(48)	2.123(3)

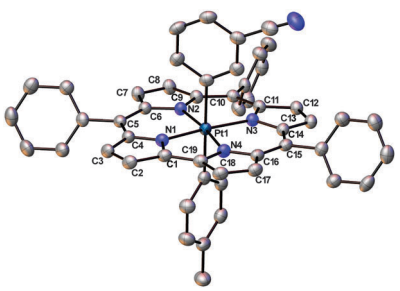

Fig. 4 Thermal ellipsoid plot for Pt(TPC)(*m*-C_6H_4CN)(*p*-$C_6H_4CH_3$) with ellipsoid probabilities at 40%. H-atoms and solvent molecules have been omitted for clarity.

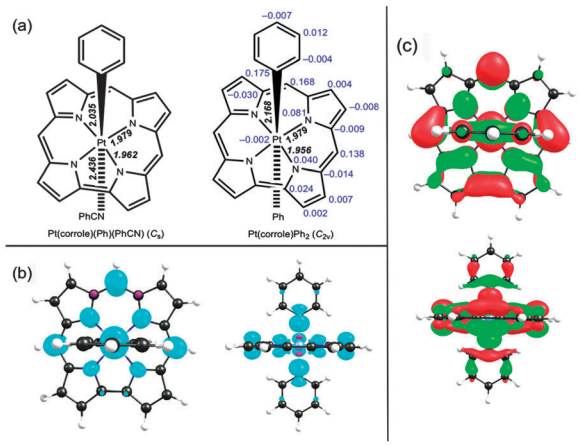

Fig. 5 Selected BP86-D3/STO-TZ2P results on the model complexes Pt(corrole)(Ph)(PhCN) (C_s) and Pt(corrole)Ph$_2$ (C_{2v}): (a) distances (black, Å) and Mulliken spin populations (blue); (b) spin density plots for Pt(corrole)Ph$_2$: top and side views; (c) the HOMO of Pt(corrole)Ph$_2$: top and side views.

in CH_2Cl_2. Note that, whereas the first oxidation potentials vary little among the different classes of metallocorroles, the reduction potentials vary considerably. Compared with Cu corroles, the Pt(IV) and Au(III) corroles undergo reduction at considerably substantially more negative potentials.[7c] Thus, Pt(IV) and Au(III) corroles exhibit relatively large electrochemical "HOMO–LUMO gaps" (*i.e.*, the algebraic difference between the first oxidation and reduction potentials) – ~1.4 eV for Pt(IV) and ~2.2 eV for Au(III). These two metal ions appear to be strongly stabilized by the trianionic corrole ligands, which would explain the resistance to reduction. In contrast, the oxidized Pt{T(*p*-X-Ph)C}(*m*-C_6H_4CN)(*p*-$C_6H_4CH_3$) complexes, like Cu triarylcorroles, are readily reduced at approximately 0.1 ± 0.1 V (*vs.* SCE), as expected on the basis of their corrole$^{\bullet 2-}$ radical character.[17]

A number of metallocorrole families such as Cu, MnCl and FeCl[15] *meso*-triarylcorroles exhibit strongly substituent-sensitive electronic absorption spectra, with the Soret maximum shifting sensitively as a function of substituents on the *meso*-aryl groups. These have been analyzed for copper triarylcorroles with TDDFT calculations and ascribed to so-called *hyper* character, *i.e.*, phenyl-to-metal charge transfer (CT) character mixing into the Soret transitions.[17] For CrO, MoO, Ag and Au triarylcorroles on the other hand the Soret maxima are relatively independent of substituents on the *meso*-aryl groups.[7c,18] Against this backdrop, the Soret maxima of Pt corroles were found to be substituent-sensitive or -insensitive, depending on the overall oxidation level of the complexes. As shown in Fig. 6 and Table 3, the Pt(IV) complexes Pt{T(*p*-X-Ph)C}(*m*-C_6H_4CN)(PhCN) exhibit substituent-insensitive Soret maxima, whereas the oxidized Pt{T(*p*-X-Ph)C}(*m*-C_6H_4CN)(*p*-$C_6H_4CH_3$) series exhibits some of the strongest *meso* substituent effects observed for metallocorroles. These observations suggest that *meso*-aryl substituent sensitivity occurs precisely in those cases where the corrole has substantial corrole$^{\bullet 2-}$ character; this is the case for Cu, FeCl, MnCl and the oxidized Pt corroles. For the other metallocorroles, where the corrole is relatively innocent, the Soret maxima are substituent-insensitive.

Compared with other 5d metallocorroles such as Au and Ir corroles, which are comparatively unreactive, platinum corroles have long been of interest on account of their potential for significant axial reactivity *vis-à-vis* small-molecule activation. Here we have presented the first unambiguous proof of platinum insertion into the corrole macrocycle, including three single-crystal X-ray structures. Two series of complexes have been prepared in low yields: the six-coordinate Pt(IV) series Pt{T(*p*-X-Ph)C}(*m*-C_6H_4CN)(PhCN) and the oxidized series Pt{T(*p*-X-Ph)C}(*m*-C_6H_4CN)(*p*-$C_6H_4CH_3$). Ongoing research on Pt corroles focuses on developing higher-yielding syntheses and on detailed studies of C–H activation and other reactivity. Whether the compounds exhibit significant biological activity, particularly anticancer activity, remains an exciting question for the future.

Table 2 Half-wave potentials *vs.* SCE ($E_{1/2}$, V) for Cu, Au and Pt {T(*p*-X-P)C} complexes in CH_2Cl_2 containing 0.1 M TBAP. Scan rate = 0.1 V s^{-1}

Complex	X	$E_{1/2ox1}$	$E_{1/2ox2}$	$E_{1/2red1}$	$E_{1/2red2}$	$E_{1/2ox1} - E_{1/2red1}$
Cu{T(*p*-X-P)C}[16]	CF_3	0.89	—	−0.08	—	0.97
	H	0.76	—	−0.20	—	0.96
	CH_3	0.70	—	−0.23	—	0.93
	OCH_3	0.65	—	−0.24	—	0.89
Au{T(*p*-X-P)C}[7c]	CF_3	0.94	—	−1.29	—	2.23
	H	0.80	1.35	−1.38	—	2.18
	CH_3	0.78	1.35	−1.42	—	2.20
	OCH_3	0.76	1.32	−1.57	—	2.33
Pt{T(*p*-X-Ph)C}(*m*-C_6H_4CN)(PhCN)	CF_3	0.72	1.40	[a]	—	[a]
	H	0.63	1.29	−0.83	—	1.46
	CH_3	0.57	1.25	−0.84	—	1.41
	OCH_3	0.53	1.14	−0.85	—	1.38
Pt{T(*p*-X-Ph)C}(*m*-C_6H_4CN)(*p*-$C_6H_4CH_3$)	CF_3	0.97	—	0.21	−0.77	0.76
	H	0.88	—	0.09	−0.82	0.79
	CH_3	0.79	—	0.03	−0.86	0.76
	OCH_3	0.74	—	0.01	−0.87	0.73

[a] Irreversible feature is noted at −1.43 eV.

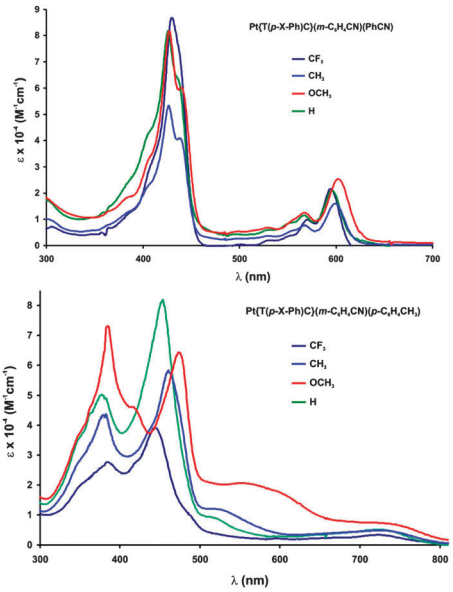

Fig. 6 Electronic absorption spectra of the Pt(IV) (top) and oxidized Pt(IV) (bottom) series.

Table 3 Soret absorption maxima (nm) of Cu, Au and Pt {T(*p*-X-P)C} complexes in CH_2Cl_2

	p-Substituent			
Complex	CF_3	H	CH_3	OCH_3
Cu[T(*p*-X-Ph)]	407	410	418	434
Au[T(*p*-X-Ph)]	419	418	420	420
Pt{T(*p*-X-Ph)C}(*m*-C_6H_4CN)(PhCN)	430	426	427	427
Pt{T(*p*-X-Ph)C}(*m*-C_6H_4CN)(*p*-$C_6H_4CH_3$)	443	453	460	475

This work was supported by the Research Council of Norway (AG), the Danish Research Council (JB) and the Advanced Light Source, Berkeley. The Advanced Light Source is supported by the Director, Office of Science, Office of Basic Energy Sciences, of the U.S. Department of Energy under Contract No. DE-AC02-05CH11231.

Notes and references

1 J. H. Palmer, *Struct. Bonding*, 2012, **142**, 49–89.
2 I. Aviv-Harel and Z. Gross, *Chem. – Eur. J.*, 2009, **15**, 8382–8394.
3 R. Padilla, H. L. Buckley, A. L. Ward and J. Arnold, *Chem. Commun.*, 2014, **50**, 2922–2924.
4 I. Nigel-Etinger, I. Goldberg and Z. Gross, *Inorg. Chem.*, 2012, **51**, 1983–1985.
5 M. K. Tse, Z. Zhang, T. C. W. Mak and K. S. Chan, *J. Chem. Soc., Chem. Commun.*, 1998, 1199–1200.
6 (*a*) J. H. Palmer, M. W. Day, A. D. Wilson, L. M. Henling, Z. Gross and H. B. Gray, *J. Am. Chem. Soc.*, 2008, **130**, 7786–7787; (*b*) J. H. Palmer, A. C. Durrell, Z. Gross, J. R. Winkler and H. B. Gray, *J. Am. Chem. Soc.*, 2010, **132**, 9230–9231.
7 (*a*) A. Alemayehu and A. Ghosh, *J. Porphyrins Phthalocyanines*, 2011, **15**, 106–110; (*b*) E. Rabinovitch, I. Goldberg and Z. Gross, *Chem. – Eur. J.*, 2011, **17**, 12294–12301; (*c*) K. E. Thomas, A. B. Alemayehu, J. Conradie, C. Beavers and A. Ghosh, *Inorg. Chem.*, 2011, **50**, 12844–12851; (*d*) K. E. Thomas, C. M. Beavers and A. Ghosh, *Mol. Phys.*, 2012, **110**, 2439–2444.
8 M. Basato, A. Biffis, G. Martinati, C. Tubaro, A. Venzo, P. Ganis and F. Benetollo, *Inorg. Chim. Acta*, 2003, **355**, 399–403.
9 The value of $A(^{195}Pt)$ used in Fig. 2 (0.8×10^{-4} cm^{-1}) is an upper limit beyond which the skewness of the large amplitude peaks becomes incorrect, resulting in shoulders on the outside of the peaks.
10 (*a*) D. Kivelson, *J. Chem. Phys.*, 1957, **27**, 1087–1098; (*b*) T. Halpern, S. M. McKoskey and J. A. McMillan, *J. Chem. Phys.*, 1970, **52**, 3526–3529; (*c*) E. F. Strother, H. A. Farach and C. P. Poole, *Phys. Rev. A: At., Mol., Opt. Phys.*, 1971, **4**, 2079–2087.
11 (*a*) J. H. Palmer, A. Mahammed, K. M. Lancaster, Z. Gross and H. B. Gray, *Inorg. Chem.*, 2009, **48**, 9308–9315; (*b*) B. Ramdhanie, J. Telser, A. Caneschi, L. N. Zakharov, A. L. Rheingold and D. P. Goldberg, *J. Am. Chem. Soc.*, 2004, **126**, 2515–2525.
12 Review: K. E. Thomas, A. Alemayehu, J. Conradie, C. M. Beavers and A. Ghosh, *Acc. Chem. Res.*, 2012, **45**, 1203–1214.
13 Copper corroles are nonplanar and an exception to this generalization: (*a*) A. B. Alemayehu, E. Gonzalez, L.-K. Hansen and A. Ghosh, *Inorg. Chem.*, 2009, **48**, 7794–7799; (*b*) A. B. Alemayehu, L.-K. Hansen and A. Ghosh, *Inorg. Chem.*, 2010, **49**, 7608–7610.
14 A. Ghosh, T. Wondimagegn and A. B. J. Parusel, *J. Am. Chem. Soc.*, 2000, **122**, 5100–5104.
15 A. Ghosh and E. Steene, *J. Inorg. Biochem.*, 2002, **91**, 423–436.
16 (*a*) I. H. Wasbotten, T. Wondimagegn and A. Ghosh, *J. Am. Chem. Soc.*, 2002, **124**, 8104–8116; (*b*) Z. Ou, J. Shao, H. Zhao, K. Ohkubo, I. H. Wasbotten, S. Fukuzumi, A. Ghosh and K. M. Kadish, *J. Porphyrins Phthalocyanines*, 2004, **8**, 1236–1247.
17 A. B. Alemayehu, J. Conradie and A. Ghosh, *Eur. J. Inorg. Chem.*, 2011, 1857–1864.
18 I. Johansen, H.-K. Norheim, S. Larsen, A. B. Alemayehu, J. Conradie and A. Ghosh, *J. Porphyrins Phthalocyanines*, 2011, **15**, 1335–1344.

